Magnetic Resonance Imaging 63 (2019) 21–28

Contents lists available at ScienceDirect

Magnetic Resonance Imaging

journal homepage: www.elsevier.com/locate/mri

Original contribution

Variation of amide proton transfer signal intensity and apparent diffusion coefficient values among phases of the menstrual cycle in the normal uterus: A preliminary study

Siyu Zhang[a], Hongzan Sun[a,*], Beibei Li[a], Xiaoqi Wang[b], Shinong Pan[a], Qiyong Guo[a]

[a] Department of Radiology, Shengjing Hospital of China Medical University, Shenyang, 110004, PR China
[b] Philips Healthcare, 7F, Tower No.2, The World Profit Centre, No.16 Tianze Road, Chaoyang District, Beijing 100600, PR China

ARTICLE INFO

Keywords:
Magnetic resonance imaging
Amide proton transfer
Apparent diffusion coefficient
Uterus
Menstrual cycle

ABSTRACT

Purpose: To explore changes in the amide proton transfer (APT) signal intensity (SI) among different phases of the menstrual cycle in healthy young women and to determine whether the APT SI correlates with the apparent diffusion coefficient (ADC).

Materials and methods: Twenty healthy women of childbearing age received regular pelvic magnetic resonance imaging (MRI) examinations and APT scans during the menstrual, proliferative and secretory phases of their menstrual cycle. Then, the APT SI and ADC values of the endometrium, myometrium and junctional zone were measured and analyzed to explore the changes during different phases of the menstrual cycle. The Pearson correlation coefficients between the APT SI and ADC were calculated.

Results: Besides the APT SI in the secretory phase, the APT SI and ADC in each menstrual phase were higher in the myometrium and endometrium than in the junctional zone, the APT Si did not differ significantly between the endometrium and myometrium during any phase. In each uterine structure, both the SI and ADC were highest in the secretory phase, second highest in the proliferative phase and lowest in the menstrual phase, but the APT SI did not differ significantly between the menstrual phase proliferative phases. Interindividual variation in APT SI and ADC for a given zone or phase ranged from 1.86% to 2.75% and from 0.37×10^{-3} mm^2/s to 0.85×10^{-3} mm^2/s, respectively. The Pearson correlation coefficient between APT SI and ADC was 0.481 ($P < 0.01$).

Conclusion: When the APT SI or ADC values are used to analyze uterine lesions, their changes during the menstrual cycle in childbearing aged women should be considered.

1. Introduction

APT imaging is a new type of chemical exchange saturation transfer (CEST) imaging technology [1,2]. By detecting low concentrations of endogenous proteins and amide chemical constituents in polypeptides, this method reflects the corresponding concentrations and environmental changes. The APT signal intensity depends on the exchange rate of amide protons and free water protons, and this exchange rate depends on the pH and protein concentration in the body [3–5]. Proliferating tumor cells produce abundant mobile proteins and peptides compared to normal tissue, leading to a higher APT SI [6]. Many studies have proven that APT SI can be used as an imaging marker to differentiate benign and malignant lesions [7–13]. Malignant lesions tend to have high APT SI. Recent studies in gynecological imaging have reported that APT SI is positively related to the pathological grade of endometrioid endometrial adenocarcinoma and cervical carcinoma [14,15].

Among MRI sequences, the T2-weighted imaging (T2WI) sequence can effectively display the structure of a normal uterus, including the myometrium (the outer myometrium), the junctional zone (the inner myometrium) and the endometrium [16]. Variation in the appearance of the uterus in different phases of the menstrual cycle can be observed with T2WI. Diffusion-weighted imaging (DWI) is a functional imaging technique that is based on the diffusion of water molecules, and the apparent diffusion coefficient (ADC) derived from DWI can reflect cell density, cellular edema and microcirculation. Studies have demonstrated that ADC values vary among different uterine structures during the different menstrual phases [17,18]. Considering the morphological

* Corresponding author at: Department of Radiology, Shengjing Hospital of China Medical University, Sanhao Street No.36, Heping District, Shenyang, Liaoning, PR China.
E-mail address: sunhongzan@126.com (H. Sun).

https://doi.org/10.1016/j.mri.2019.07.007
Received 27 January 2019; Accepted 13 July 2019

changes observed in T2WI and the variation of ADC values in various uterine structures during the menstrual cycle, physiological changes may cause corresponding variation in the APT signal intensity and, thus, could affect the baseline APT SI used to assess uterine abnormalities. Therefore, by evaluating how APT SI and ADC differed among different uterine structures based on T2WI during different phases in the menstrual cycle in childbearing aged women, this study evaluated whether APT SI changes during different menstrual phases in the normal uterus and whether APT SI correlates with ADC.

2. Materials and methods

2.1. Healthy volunteer study

This Institutional Review Board approved this study, and every group of volunteers provided written informed consent before examination. From December 2017 to March 2018, 20 healthy women of childbearing age were enrolled; their mean age was 24.2 ± 0.49 years (24–26 years). The inclusion criteria included the following: (1) healthy young women, from 18 to 35 years old; (2) a regular menstrual cycle, ranging from 28 to 35 days. The exclusion criteria were as follows: (1) systemic diseases, such as heart disease and kidney disease; (2) history of menorrhalgia; (3) history of oral contraceptive or estrogen use; (4) history of childbearing, or intrauterine contraceptive ring; (5) history of gynecological diseases; and (6) contraindications to MRI, such as metal implants, cardiac pacemakers and claustrophobia. MRI was performed at 3 time points in a normal menstrual cycle for each volunteer: the menstrual phase (first to fourth day of menstruation), the proliferative phase (six to fourteen days after menstruation) and the secretory phase (eighteen to twenty-eight days after menstruation). All participants were required to record their daily basal body temperature, length of the menstrual cycle and each menstrual phase in the first 6 month of the examination, as show in Table 1. The rules use to define the menstrual phases were: The proliferative phase is from the end of menstruation to ovulation, and the secretory phase is from ovulation to before the first day of the next cycle, the date of ovulation was estimated on the basis of elevated basal body temperature. The timing of the MRI examinations was determined by reference to the average menstrual cycle in the first 6 months of the examination and the basal body temperature.

Table 1
Average lengths of the menstrual cycle and each menstrual phases in the first 6 months.

Participant	Length of the menstrual cycle(d)	Length of the menstrual phase(d)	Length of the proliferative phase(d)	Length of the secretory phase(d)
1	28	5	9	14
2	29	4	11	14
3	30	6	9	15
4	28	4	10	14
5	31	5	12	14
6	29	5	11	13
7	32	7	10	15
8	30	7	9	14
9	29	5	10	14
10	29	5	10	14
11	28	5	9	14
12	31	6	10	15
13	30	7	8	15
14	30	7	9	14
15	28	5	9	14
16	34	7	12	15
17	28	4	10	14
18	28	4	11	13
19	29	4	12	13
20	33	6	12	15
	29.7	5.4	10.2	14.15

2.2. MR imaging protocol

Volunteers underwent MRI in a Philips 3.0-T unit (Ingenia 3.0 T CX; Philips HealthTech, Best, the Netherlands). Interleaved dual RF transmit coils were applied in APT (0.5 s for each turn) with no interval between shifting RF coils to provide a longer amide proton saturation effect (2 s) at the same time limiting the RF load on transmit coils; dual RF transmit coils were also used for other MRI protocols but to achieve a more homogeneous B1 field; the dS Torso coil was used in addition to embedded coils. Axial T1WI, T2WI and DWI uterine images were acquired and examined to exclude anatomical abnormalities in the test subjects, followed by APT imaging.

APT imaging was performed with an amide proton saturation pulse of 2 s duration (a combination of 4 consecutive 0.5-second sinc-Gauss-shaped elements interleaved with RF transmit coils) and a saturation power level corresponding to the B1 root mean square (B1, rms) of 2.0 mT. To acquire APT z-spectrum before B0 correction and APT calculation, the imaging was repeated with 6 saturation frequency offsets (+3.5 ppm, −3.5 ppm, +3.5 ± 0.8 ppm and −3.5 ± 0.8 ppm, the other side of APT z-spectrum was acquired to compensate for the MT effect) from the water frequency. Off-resonance correction was applied by the measurement of the B0 map using 3 sets of 3D turbo spin echo (TSE) sequence with identical spatial resolution but with shifted echo times (0.4 msec for the change in echo time, acquired at 3.5 ppm to enhance image signal-to-noise ratio at 3.5 ppm).

The accuracy of APT depends largely on B0 homogeneity to calculate the CEST effect. The updated APT method utilizes 3D mDIXON TSE to estimate the B0 map and improve the APT measurement.

Axial DWI was performed with b values of 0, 100 and 800, with an average of 2, 2 and 4, respectively, for each b value, and an ADC map was generated based on the DWI images. We added b = 100 for diffusion measurements to reduce the capillary perfusion effect in small b value ranges in ADC quantification, according to intravoxel incoherent motion references.

The other MRI parameters used for APT, DWI, T1WI and T2WI are summarized in Table 2.

2.3. Image and data analysis

The acquired APT raw data were imported into the IDL software (Research Systems Inc., Boulder, Colorado) for analysis. Two radiologists independently interpreted MRI images: one radiologist with twenty years of experience in abdomen imaging and another radiologist with eleven years of experience in gynecological imaging. They were blinded to the volunteers' information and the menstrual phase. First, they identified the myometrium, endometrium and junctional zone by T2WI and DWI. Second, each reader drew two regions of interest (ROIs) on the corresponding zonal structures located on the T2WI and DWI using a freehand tool. The ROIs were then copied to the corresponding APT source image and the ADC map to obtain the mean APT SI and mean ADC. The two ROIs were measured, and the average value was used to reduce random variability in the measurements. For the myometrium and junctional zone, one ROI was placed on the left wall and another on the right wall, as shown in Figs. 1–3. The ROIs were selected to be as large as possible but to not include areas affected by susceptibility artifacts. Third, the radiologists recorded the mean APT SI and the mean ADC of the ROIs in the myometrium, endometrium and junctional zone. The mean of the two readers' APT SI and ADC values were used for the final analysis.

2.4. Statistical analysis

SPSS 22 software was used for statistical analysis of the data. The data were tested for normality using Shapiro-Wilks test ($P > 0.05$ for the APT SI and ADC of each uterine structure in each phase) and are described as the mean ± standard deviation (SD) (Table 3). We

Table 2
Details of MRI parameters.

Parameter	APT	DWI	T1WI	T2WI
Imaging technique	3D[c] Multishot TSE[d]	Single-shot EPI	MS TSE	MS MultiVane TSE
Repetition time/echo time (msec)	6294/5.9	3500/75	400/8	3000/100
Flip angle (degree)	90	90	90	90
Field of view (mm^2)	230 × 355	300 × 218	200 × 200	200 × 200
Matrix (frequency × phase)	116 × 177	100 × 72	268 × 200	200 × 200
Spatial resolution (mm^2)	2.0 × 2.0	3.0 × 3.0	0.75 × 1	1.0 × 1.0
Section thickness (mm)	5	4	4	4
Section gap (mm)	N/A[g]	2	0.4	0.4
No. of sections	9	20	24	24
No. of signals acquired	2	2	1	1
ETL[a] (TSE factor)	158	N/A	4	24
EPI[b] factor	N/A	35	N/A	N/A
Acquisition acceleration	3 (SENSE[e])	3 (SENSE)	4 (CS-SENSE)	2 (SENSE)
Fat suppression	SPAIR[f]	SPAIR	No	No
Total imaging time (m:s)	05:46	04:44	01:17	01:18

[a] ETL: echo train length.
[b] EPI: echo planar imaging.
[c] 3D: three-dimensional.
[d] TSE: turbo spin echo.
[e] SENSE: sensitivity encoding.
[f] SPAIR: spectral attenuation with inversion recovery.
[g] N/A: not applicable.

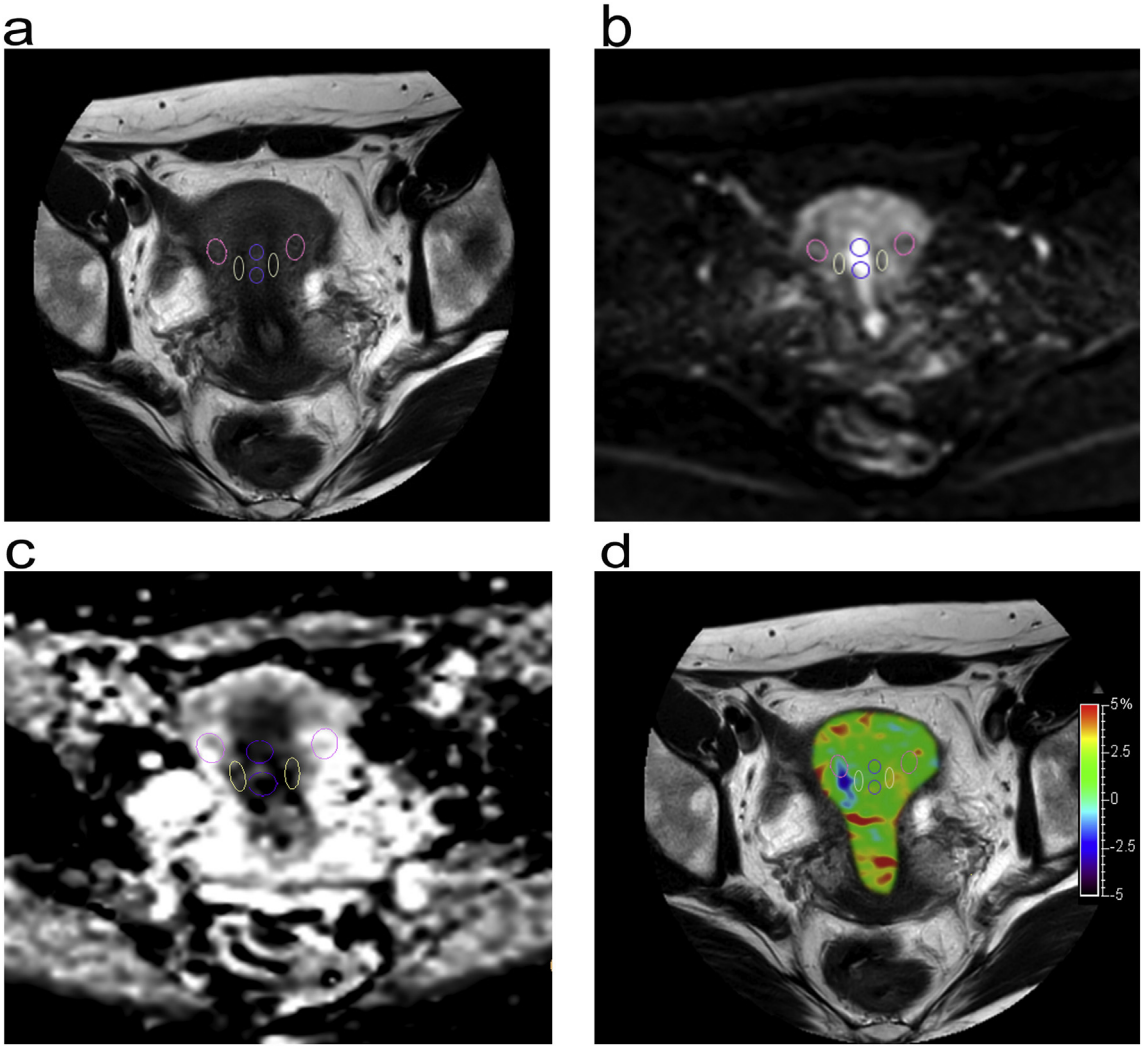

Fig. 1. Images in a 24-year-old woman with mensrual phase. Images from T2WI (a) and DWI (b = 800) (b) were the reference for selection of ROIs. The ROIs were then copied to the corresponding ADC map (c) and APT pseudo color image (d).

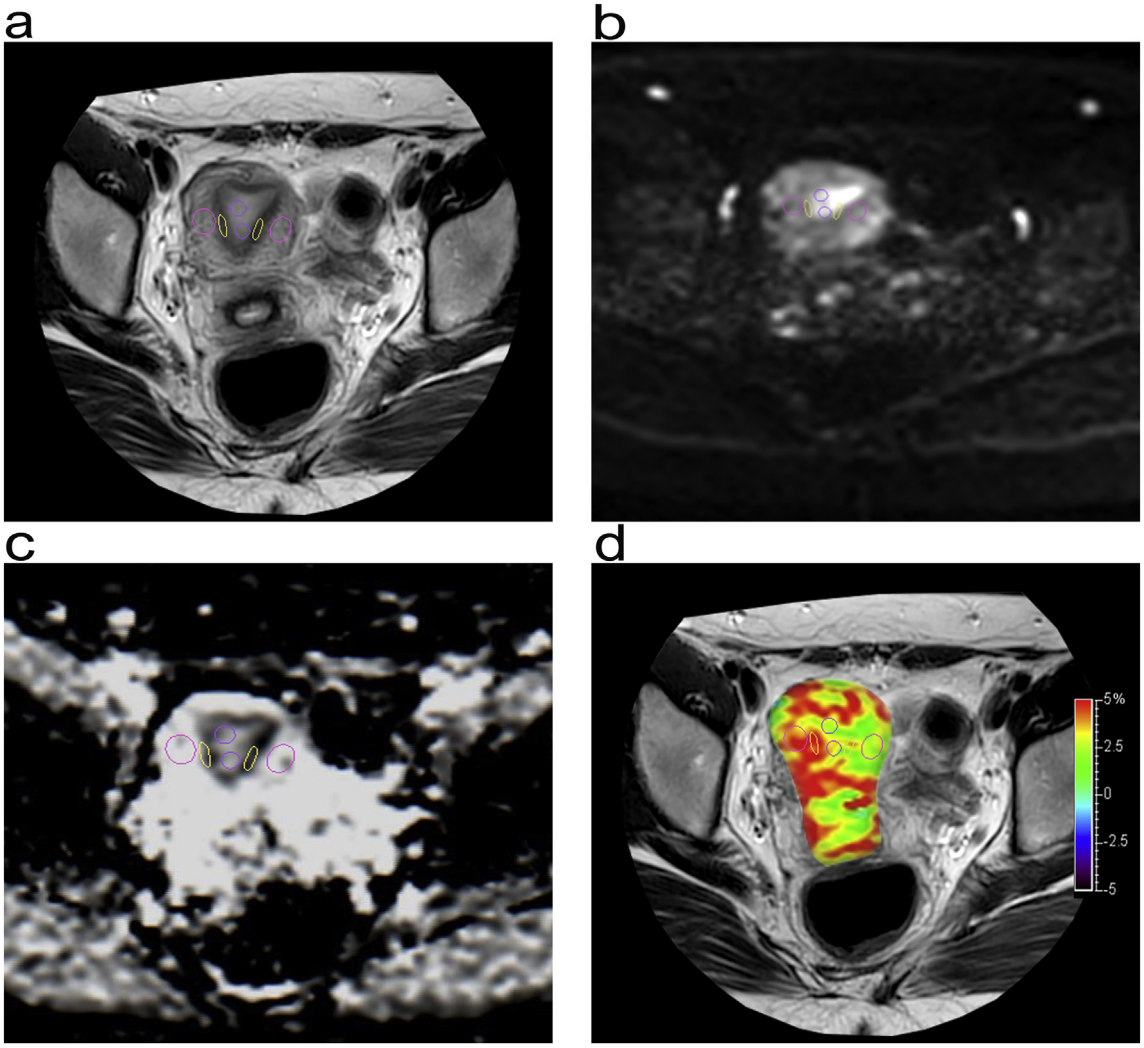

Fig. 2. Images in the same participant with proliferative phase. Images from T2WI (a) and DWI (b = 800) (b) were the reference for selection of ROIs. The ROIs were then copied to the corresponding ADC map (c) and APT pseudo color image (d).

calculated the intraclass correlation coefficient using a two-way random-effects model to describe the correlations between APT SI and ADC values of the two readers based on the following criteria: < 0.40, poor agreement; 0.40–0.59, fair agreement; 0.60–0.74, good agreement; and greater than or equal to 0.75, excellent agreement.

Single-factor ANOVA was used to compare the APT SI and ADC of different uterine structures during the same menstrual phase. Then, the least-significant difference (LSD) test was used for multiple comparisons of APT SI and ADC among the three uterine structures; $P < 0.05$ indicated statistical significance. Multiple-factor repeated measures ANOVA was used to compare differences in the APT SI and ADC among different menstrual phases for the same uterine structure; $P < 0.05$ indicated statistical significance. The intraindividual difference, which is the difference between the maximum and minimum APT SI or ADC values over the three menstrual phases for each participant, was calculated. In addition, the interindividual variation in the APT SI or ADC values for each zone and phase was calculated. The Pearson correlation analysis was used to measure correlation between APT SI and ADC.

3. Results

3.1. Intraclass correlation coefficients between two readers

The intraclass correlation coefficients between the two readers of APT SI and t ADC values of each zonal structure during each menstrual phase are summarized in Table 4. All APT SI and ADC values had fair, good or excellent interobserver agreement.

3.2. Differences in APT SI and ADC values among uterine structures during the same menstrual phase

During each of the three phases, the APT SI differed significantly among the structures of the uterus ($P < 0.001$) (Table 3). The APT SI of the endometrium and the outer myometrium was higher, whereas that of the junctional zone was the lowest. The APT SI differed significantly between the junctional zone and the endometrium and between the junctional zone and the myometrium during the three phases ($P < 0.05$). However, the APT SI did not differ significantly between the endometrium and myometrium during any phase ($P > 0.05$).

The ADC of the uterine structures also varied significantly during the three phases ($P < 0.001$). In the same menstrual phase, the different uterine structures had significantly different ADC values ($P < 0.001$) (Table 3). The ADC values of the uterus were highest in the myometrium, second highest in the endometrium and lowest in the junctional zone. The APT SI and ADC values of the uterine structures during the three menstrual phases are shown in Fig. 4.

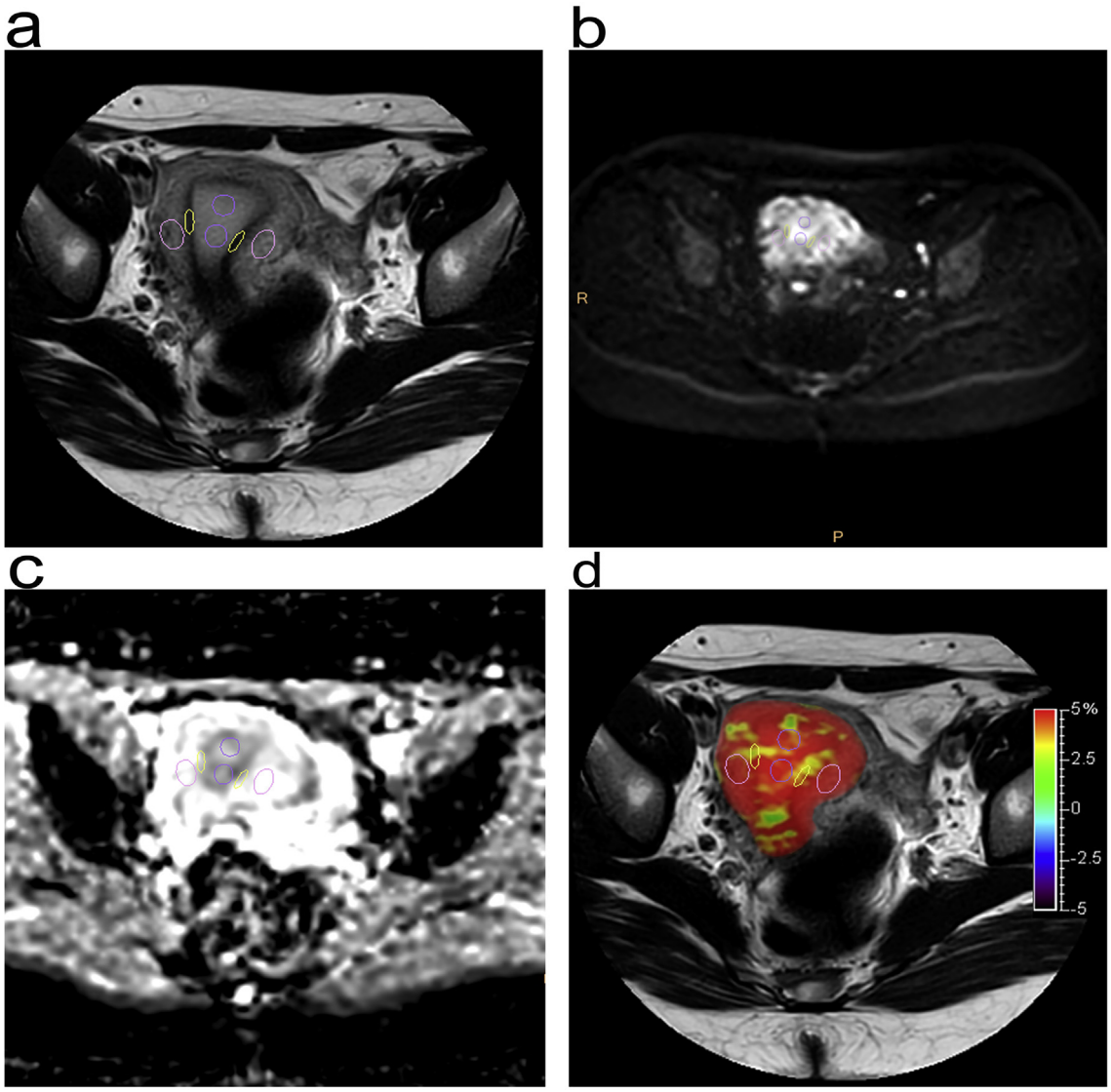

Fig. 3. Images in the same participant with secretory phase. Images from T2WI (a) and DWI (b = 800) (b) were the reference for selection of ROIs. The ROIs were then copied to the corresponding ADC map (c) and APT pseudo color image (d).

3.3. Differences in the APT SI and ADC values among menstrual phases for each uterine structure

An intergroup difference was observed in the APT SI among the different uterine structures ($P < 0.001$), and an intragroup difference was observed among the menstrual phases for the same uterine structure ($P < 0.001$); no interaction was observed between the menstrual phase and the uterine structure ($P = 0.498$) (Table 5). APT SI did not differ significantly between the menstrual and proliferative phases ($P > 0.05$) but differed significantly between the menstrual and secretory phases as well as between the proliferative and secretory phases ($P < 0.05$). As shown in Fig. 4, the APT SI of all uterine structures in the secretory phase was significantly higher than that in the menstrual and proliferative phases.

Table 3
Averages and SDs of APT SIs and ADC values of each zonal structure during each menstrual phase with pairwise comparisons.

	Endometrium (1)	Myometrium (2)	Junctional zone (3)	F	P^b	*P* value (1 vs 2)	*P* value (1 vs 3)	*P* value (2 vs 3)
APT SIs (%)								
Menstrual phase	3.16 ± 0.54[a]	3.41 ± 0.59	2.61 ± 0.54	10.69	< 0.001	0.16	0.03	0.00
Proliferative phase	3.34 ± 0.76	3.57 ± 0.62	2.81 ± 0.62	6.89	< 0.001	0.27	0.01	0.01
Secretory phase	4.26 ± 0.65	4.09 ± 0.61	3.40 ± 0.71	9.74	< 0.001	0.41	0.00	0.02
ADC values ($\times 10^{-3}$ mm^2/s)								
Menstrual phase	0.94 ± 0.15	1.50 ± 0.19	0.84 ± 0.10	109.69	< 0.001	< 0.001	< 0.001	< 0.001
Proliferative phase	1.35 ± 0.15	1.70 ± 0.18	0.97 ± 0.09	127.41	< 0.001	< 0.001	< 0.001	< 0.001
Secretory phase	1.39 ± 0.16	1.74 ± 0.15	0.98 ± 0.17	111.33	< 0.001	< 0.001	< 0.001	< 0.001

[a] Unless otherwise indicated, data are the mean ± SD.
[b] *P* values < 0.05 were considered to indicate a significance difference.

Table 4
Intraclass correlation coefficients between two readers of the APT SIs and ADC values of each zonal structure during each menstrual phase.

	Menstrual phase	Proliferative phase	Secretory phase
APT SIs			
Endometrium	0.72 (0.43, 0.88)[a]	0.81 (0.57, 0.91)	0.85 (0.67, 0.94)
Myometrium	0.67 (0.33, 0.85)	0.58 (0.19, 0.81)	0.63 (0.28, 0.84)
Junctional zone	0.62 (0.27, 0.83)	0.88 (0.73, 0.95)	0.91 (0.79, 0.96)
ADC values			
Endometrium	0.78 (0.55, 0.91)	0.83 (0.62, 0.93)	0.78 (0.40, 0.87)
Myometrium	0.89 (0.75, 0.96)	0.86 (0.68, 0.94)	0.79 (0.54, 0.91)
Junctional zone	0.45 (0.13, 0.74)	0.41 (0.005, 0.71)	0.43 (−0.005, 0.73)

[a] The data points are the intraclass correlation coefficient (95% confidence interval [CI]).

An intergroup difference was observed in the ADC values among different uterine structures ($P < 0.001$) and also among the menstrual phases for the same uterine structure ($P < 0.001$). A significant interaction was found between the menstrual cycle and the uterine structure ($P < 0.001$); that is, the relationship between the uterine structures and their ADC values was modified by the menstrual phase (Table 5). Fig. 4 shows that the ADC values were lowest in the menstrual phase, second highest in the proliferative phase and highest in the secretory phase.

Intraindividual variation of the APT SI over the three menstrual phases was 1.56 ± 0.64 (%) for the endometrium, 1.08 ± 0.61 (%) for the myometrium and 1.27 ± 0.64 (%) for the junctional zone, whereas that of ADC values was 0.51 ± 0.21 ($\times 10^{-3}$ mm^2/s) for the endometrium, 0.33 ± 0.21 ($\times 10^{-3}$ mm^2/s) for the myometrium and 0.27 ± 0.12 ($\times 10^{-3}$ mm^2/s) for the junctional zone. The interindividual maximum–minimum APT SI and ADC value differences among the twenty participants for each uterine zone and menstrual phase are shown at Table 6.

3.4. Correlations between APT SI and ADC values

The Pearson correlation coefficient between APT SI and ADC was 0.481 ($P < 0.01$). The Pearson correlation coefficients between APT SI and ADC in the menstrual phase, proliferative phase and secretory phase were 0.414 ($P = 0.01$), 0.408 ($P = 0.01$) and 0.475 ($P < 0.01$), respectively. The Pearson correlation coefficients between APT SI and ADC in the endometrium, junctional zone and myometrium were 0.380 ($P = 0.03$), 0.419 ($P = 0.01$) and 0.193 ($P = 0.139$), respectively.

Table 5
Multiple-factor repeated measures ANOVA of the APT SIs and ADC values of each zonal structure during each menstrual phase.

Source of variation	APT SI		ADC value	
	F	P[a]	F	P
Uterine structure	22.913	< 0.001	293.563	< 0.001
Menstrual phase	32.313	< 0.001	63.682	< 0.001
Uterine structure × menstrual phase	0.874	0.498	7.074	< 0.001

[a] P values < 0.05 were considered to indicate a significance difference.

4. Discussion

Amide proton transfer imaging is a newly emerged molecular imaging technique that can differentiate among different uterine structures and tends to vary by the phase of the menstrual cycle similar to the ADC. Our study found a moderate correlation between APT SI and ADC. The APT SI reveals protein concentration; ADC values primarily reflect cell density. Thus, moderate correlation between APT SI and ADC is reasonable because protein concentration and cell density are both increased by cell proliferation.

The changes in APT SI and ADC values seen during the menstrual cycle may reflect periodic physiological changes in different uterine structures. The endometrium contains abundant extracellular free proteins and peptides. These proteins are expressed in the proliferative and secretory phases, and epithelial cells in the endometrium express significantly higher protein levels during the secretory phase than during the proliferative phase [19,20]. The APT SI is positively correlated with the protein concentration. Therefore, the APT SI of the endometrium was highest in the secretory phase. The presence of blood in the cavity could be related to lower ADC values in the menstrual phase. In the proliferative phase and secretory phases, myometrial edema could be associated with higher APT SI similar to the higher APT SI seen in brain edema [21]. In addition, this myometrial edema could also be associated with higher ADC. Previous studies have shown that the water content of the uterine junctional zone was the lowest of the three structures. Additionally, its muscle cell structure density was higher than that in the other regions; the cytoplasmic nuclear ratio was low, and the junctional zone was found to be the structure primarily involved in regulating the contraction of the non-pregnant uterus. Smooth muscle cell contraction and other factors all resulted in a lower APT SI and ADC in the junctional zone [22].

In addition, we found that the APT SI of each structure during the

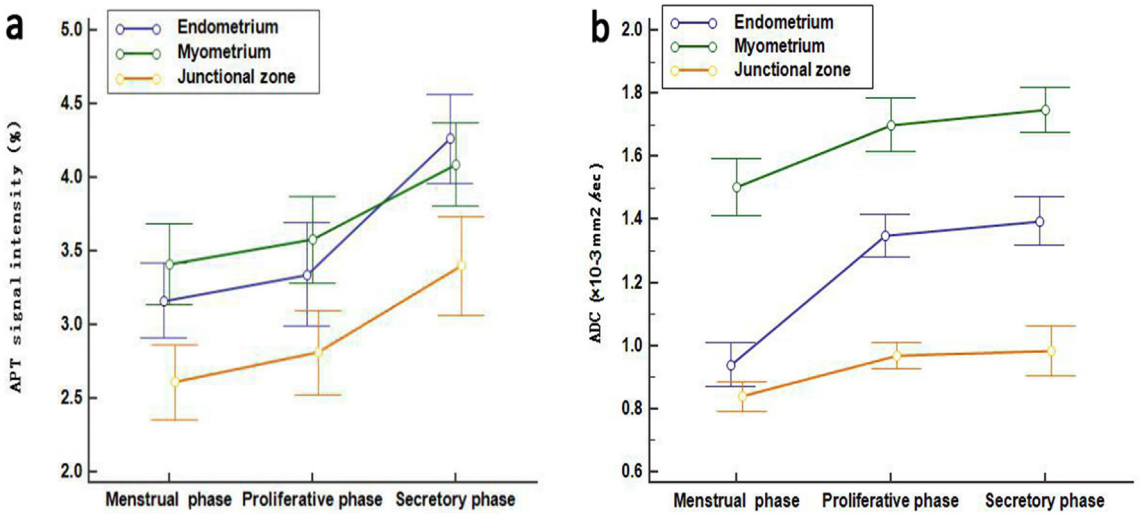

Fig. 4. Changes in APT Sis (a) and ADCs (b) of endometrium, myometrium and junctional zone during three different menstrual cycles. The data points and error bars were the mean values and the 95% confidence interval.

Table 6
Inerindividual maximum-minimum APT SI and ADC difference for a given zone and phase.

	APT SI (%)			ADC value($\times 10^{-3}$ mm^2/s)		
	Menstrual phase	Proliferative phase	Secretory phase	Menstrual phase	Proliferative phase	Secretory phase
Endometrium	1.29	1.75	1.95	0.66	0.49	0.62
Myometrium	2.46	2.3	1.86	0.85	0.54	0.53
Junctional zone	2.03	1.86	2.35	0.38	0.37	0.74

secretory phase was significantly higher than that during the proliferative and menstrual phase; the differences among these APT SIs was more marked than that among ADC values because APT imaging is related to the protein concentration and is more direct and intuitive. The mid-secretive phase is the period with the highest endometrial receptivity, namely, the 'optimal fertilization window', and many highly expressed proteins may be associated with this endometrial receptivity and embryo implantation [23]. Therefore, the secretory phase is the most critical phase for evaluation of uterine function, and infertility or functional abortions may be associated with a lower protein concentration during the secretory phase. Our results suggest that APT imaging is an effective method for evaluating the function of the uterus in vivo with significant advantages over other MRI methods, such as DWI.

We observed changes in both APT SI (from 1.1% to 1.6% on average) and ADC (from 0.25×10^{-3} mm^2/s to 0.55×10^{-3} mm^2/s on average) over the three menstrual phases of the normal uterus. The APT SI of the secretory phase was higher than that of the other cycle phases; this phase related difference was most marked in the endometrium. The differences in APT SI observed in different menstrual phases are meaningful for the interpretation of APT SI in tumor imaging. The difference in APT SI between benign and malignant lesions ranges from 1.3% to 3.2% [9,24], which is comparable to the variation in the APT SI of the normal uterus during the three menstrual phases in our study. Similarly, the difference in ADC values between malignant and non-malignant uterine lesions ranges from 0.4×10^{-3} mm^2/s to 0.65×10^{-3} mm^2/s [25,26], which is also comparable to the variation in the ADC values in our study. This result is similar to those of the study of Kido et al. [18]. This overlap may be particularly problematic when using APT SI or ADC values as imaging markers for diagnosing uterine diseases. Therefore, in clinical practice, we should consider the menstrual cycle when interpreting APT SI and ADC values. Uterine lesions occur most often in the endometrium or myometrium. In these structures, APT SI tends to increase during secretion and ADC tends to decrease during menstruation. Therefore, it is better to avoid using APT SI measurements obtained during the secretory phase and instead use ADC measurements obtained during the menstrual phase to reduce the impact of menstrual cycle related variation on baseline APT SI and ADC values.

Our research has some limitations to. First, menstrual cycles were not accurately determined by detecting the levels of estrogen and progesterone in the serum of the subjects. However, the participants' menstrual cycle records and rules for defining the menstrual phases may have reduced this error. Second, error may have resulted from the ROI delineation, with different ROIs leading to different results. This study did not take into account how the ROI affected the measured values, and only the largest possible ROI was used as a drawing standard, which may have caused measurement error. Finally, many problems remain to be solved in APT imaging technology, such as addressing the direct water saturation effect and magnetization transfer; enhancing the signal; improving the image quality; determining the appropriate scanning time, energy and turn angle of the bias RF pulse; and reducing motion and shadow artifacts.

5. Conclusion

We observed variation in APT SI and ADC values in the normal uterus during different menstrual phases; the range of that variation is comparable to the range of variation in benign and malignant lesions. Therefore, when using the APT SI or ADC to analyze uterine lesions, the variation of these values with the menstrual cycle in childbearing aged women should be considered.

Acknowledgements

We thank Philips Healthcare for supporting this study.

Funding

This work was supported by grants from the National Key Research and the Development Program of China (No. 2016YFC0107102).

References

[1] Zhou J, Lal B, Wilson DA, Laterra J, van Zijl PC. Amide proton transfer (APT) contrast for imaging of brain tumors. Magn Reson Med 2003;50(6):1120–6.
[2] Schmidt H, Schwenzer NF, Gatidis S, Kustner T, Nikolaou K, Schick F, et al. Systematic evaluation of amide proton chemical exchange saturation transfer at 3 T: effects of protein concentration, pH, and acquisition parameters. Invest Radiol 2016;51(10):635–46.
[3] Zhou1 J, Payen J-F, Wilson DA, Traystman RJ, van Zijl PCM. Using the amide proton signals of intracellular proteins and peptides to detect pH effects in MRI. Nat Med 2003;9(8):1085–90.
[4] Yan K, Fu Z, Yang C, Zhang K, Jiang S, Lee DH, et al. Assessing amide proton transfer (APT) MRI contrast origins in 9 L gliosarcoma in the rat brain using proteomic analysis. Molecular imaging and biology: MIB: the official publication of the Academy of Molecular Imaging 2015;17(4):479–87.
[5] Zhou J, Wilson DA, Sun PZ, Klaus JA, Van Zijl PC. Quantitative description of proton exchange processes between water and endogenous and exogenous agents for WEX, CEST, and APT experiments. Magn Reson Med 2004;51(5):945–52.
[6] Jones CK, Schlosser MJ, van Zijl PCM, Pomper MG, Golay X, Zhou J. Amide proton transfer imaging of human brain tumors at 3T. Magn Reson Med 2006;56(3):585–92.
[7] Zou T, Yu H, Jiang C, Wang X, Jiang S, Rui Q, et al. Differentiating the histologic grades of gliomas preoperatively using amide proton transfer-weighted (APTW) and intravoxel incoherent motion MRI. NMR Biomed 2018;31(1).
[8] Yu L, Li C, Luo X, Zhou J, Zhang C, Zhang Y, et al. Differentiation of malignant and benign head and neck tumors with amide proton transfer-weighted MR imaging. Mol. Imaging Biol. 2019;21(2):348–55.
[9] Ohno Y, Yui M, Koyama H, Yoshikawa T, Seki S, Ueno Y, et al. Chemical exchange saturation transfer MR imaging: preliminary results for differentiation of malignant and benign thoracic lesions. Radiology 2016;279(2):578–89.
[10] Nishie A, Takayama Y, Asayama Y, Ishigami K, Ushijima Y, Okamoto D, et al. Amide proton transfer imaging can predict tumor grade in rectal cancer. Magn Reson Imaging 2018;51:96–103.
[11] Choi YS, Ahn SS, Lee SK, Chang JH, Kang SG, Kim SH, et al. Amide proton transfer imaging to discriminate between low- and high-grade gliomas: added value to apparent diffusion coefficient and relative cerebral blood volume. Eur Radiol 2017;27(8):3181–9.
[12] Joo B, Han K, Choi YS, Lee SK, Ahn SS, Chang JH, et al. Amide proton transfer imaging for differentiation of benign and atypical meningiomas. Eur Radiol 2018;28(1):331–9.
[13] Park JE, Kim HS, Park KJ, Choi CG, SJ K. Histogram analysis of amide proton transfer imaging to identify contrast-enhancing low-grade brain tumor that mimics high-grade tumor: increased accuracy of MR perfusion. Radiology 2015;277(1):151–61.
[14] Takayama Y, Nishie A, Togao O, Asayama Y, Ishigami K, Ushijima Y, et al. Amide proton transfer MR imaging of endometrioid endometrial adenocarcinoma: association with histologic grade. Radiology 2018;286(3):909–17.
[15] Li B, Sun H, Zhang S, Wang X, Guo Q. Amide proton transfer imaging to evaluate the grading of squamous cell carcinoma of the cervix: a comparative study using

18F FDG PET. J Magn Reson Imaging;0(0).
[16] Haynor DR, Mack LA, Soules MR, Shuman WP, Montana MA, Moss AA. Changing appearance of the normal uterus during the menstrual cycle: MR studies. Radiology 1986;161(2):459–62.
[17] Lyng H, Haraldseth O, Rofstad EK. Measurement of cell density and necrotic fraction in human melanoma xenografts by diffusion weighted magnetic resonance imaging. Magn Reson Med 2000;43(6):828–36.
[18] Kido A, Kataoka M, Koyama T, Yamamoto A, Saga T, Togashi K. Changes in apparent diffusion coefficients in the normal uterus during different phases of the menstrual cycle. Br J Radiol 2010;83(990):524–8.
[19] Huang HY, Chan SH, Yu HT, Wang HS, Lai CH, Soong YK. Interleukin-18 system messenger RNA and protein expression in human endometrium during the menstrual cycle. Fertil Steril 2006;86(4):905–13.
[20] Baek W-K, Kim D, Jung N, Yi Y-W, Kim JM, Cha S-D, et al. Increased expression of cyclin G1 in leiomyoma compared with normal myometrium. Am J Obstet Gynecol 2003;188(3):634–9.
[21] Yu H, Lou H, Zou T, Wang X, Jiang S, Huang Z, et al. Applying protein-based amide proton transfer MR imaging to distinguish solitary brain metastases from glioblastoma. Eur Radiol 2017;27(11):4516–24.
[22] Scoutt L, Flynn S, Luthringer D, McCauley T, McCarthy S. Junctional zone of the uterus: correlation of MR imaging and histologic examination of hysterectomy specimens. Radiology 1991;179(2):403–7.
[23] Soares Lopes IMR, Pinheiro Baracat MC, JesusSimões M, SantosSimões R, Baracat EC, Soares JM. Endometrium in women with polycystic ovary syndrome during the window of implantation. Revista da Associação Médica Brasileira (English Edition) 2011;57(6):688–95.
[24] Law BKH, King AD, Ai QY, Poon DMC, Chen W, Bhatia KS, et al. Head and neck tumors: amide proton transfer MRI. Radiology 2018;288(3):782–90.
[25] Tamai K, Koyama T, Saga T, Morisawa N, Fujimoto K, Mikami Y, et al. The utility of diffusion-weighted MR imaging for differentiating uterine sarcomas from benign leiomyomas. Eur Radiol 2008;18(4):723–30.
[26] Tamai K, Koyama T, Saga T, Umeoka S, Mikami Y, Fujii S, et al. Diffusion-weighted MR imaging of uterine endometrial cancer. Journal of magnetic resonance imaging: JMRI 2007;26(3):682–7.